Journal of Molecular Structure 1142 (2017) 66–72

Contents lists available at ScienceDirect

Journal of Molecular Structure

journal homepage: http://www.elsevier.com/locate/molstruc

Photoresponse and DFT studies of new synthesized 2-benzylidene-3-hydroxy -1-(5,6-diphenyl-1,2,4-triazine-3-yl) hydrazine and optical sensor application

A. Taha [a], A.A.M. Farag [b, c, *], O.M.I. Adly [a], N. Roushdy [d], Magdy Shebl [a], H.M. Ahmed [a]

[a] Chemistry Department, Faculty of Education, Ain Shams University, Roxy, Cairo, Egypt
[b] Physics Department, Faculty of Science and Arts, Aljouf University, Saudi Arabia
[c] Thin Film Laboratory, Physics Department, Faculty of Education, Ain Shams University, Roxy, Cairo, Egypt
[d] Electronic Materials Department, Advanced Technology and New Material Institute, City for Scientific Research and Technological Applications, New Borg El Arab City, 21934, Alexandria, Egypt

ARTICLE INFO

Article history:
Received 15 February 2017
Received in revised form
9 April 2017
Accepted 10 April 2017
Available online 12 April 2017

Keywords:
Schiff base
Density function (DFT)
Optical characteristics
Current-voltage characteristics

ABSTRACT

A newly Schiff base,2-benzylidene-3-hydroxy-1-(5,6-diphenyl-1,2,4-triazine-3-yl)hydrazine] (HBDHT) was synthesized and characterized on the basis of micro-analytical and spectroscopic studies. Basic parameters of the combined compound HBDHT were ascertained on the premise of DFT level actualized on *Gaussian 09*. Thin films of HBDHT were successfully prepared by spin coating technique and confirmed by atomic force microscopy (AFM). The optical attributes of the studied films were considered utilizing spectrophotometric estimations in a wide spectral range of 200–2500 nm. Some important optical parameters such as extinction index, refractive index, dispersion energy, oscillator energy and high-frequency dielectric constant were extracted. Analysis of the absorption coefficient near the fundamental absorption edge confirms an indirectly allowed transition with an energy gap of 1.7eV. The refractive index dispersion was estimated on basis of single oscillator model expressed by Wemple –Didomenico. Current–voltage (*I–V*) characteristics were studied in dark and under illumination of 100 mW/cm^2 to clarify the sensitivity to light. Moreover, the photo-transient properties were also investigated to confirm that the prepared heterojunction based HBDHT can be operated as a photodiode.

1. Introduction

Triazine and its subordinates, has numerous applications from manufacturing usage, to scholarly interests which may one day work out as expected as pharmaceutically viable molecules particles. These compounds can create supermolecular structures through correlative varieties of hydrogen-bonding sites [1–6]. 1,2,4-Triazines and their derivatives are found to possess a wide variety of pesticide or herbicide components in agriculture, pharmacological and medicinal activities [7–9]. In addition, Schiff base macro-ligands derived from 1, 2, 4-triazine derivatives have traditionally found application in analytical chemistry such as complexing agents [10]. Likewise, various compounds, characterized by π-conjugation were considered as a candidate for charge directing materials because of their interesting chemical and electrical characteristics. So far, π-conjugated macromolecular have been broken mainly as π-type materials, giving rise to a somewhat unbalanced development causing differences in the efficiency between the hole- and electron-transporting materials which favor the aromaticity and electric conductivity [11]. This hence focuses on the compound namely, *2-benzylidene-3-hydroxy-1-(5, 6-diphenyl-1,2,4-triazine-3-aryl)hydrazine* (HBHDT). Our main aim is the study of the variation of some electronic properties related with the electron conduction of the synthesized 1,2,4-triazine Schiff base compound [12]. The structure of that compound has been illustrated by essential analysis and spectral studies. Furthermore, crystalline and topography properties are described by AFM. Moreover, photoluminescence and optical absorption characteristics of the films are investigated as well. As further support to our experimental work, molecular orbital calculations have been accomplished to deduce structural parameters by means of a density function (DFT) at the B3LYP-6-31G level implanted by the *Gaussian 09* program. Moreover, the dark current density–voltage

* Corresponding author. Thin Film Laboratory, Physics Department, Faculty of Education, Ain Shams University, Roxy, Cairo, Egypt.
E-mail address: alaafaragg@gmail.com (A.A.M. Farag).

http://dx.doi.org/10.1016/j.molstruc.2017.04.025
0022-2860/

characteristics were also studied to realize the prime parameters of the prepared hetero-junction to investigate the sensitivity for photodiodes applications.

2. Experimental

2.1. Materials and methods

All chemicals were of reagent grade and used as commercially purchased without further purification except dioxane which purified using the standard methods [13,14]. Buffer and potassium hydroxide solutions were prepared and standardized by the recommended methods [15]. FT-IR spectrum of the present compound was recorded in the range of 400–4000 cm^{-1} with an FT-IR–8101 Shimadzu spectrometer using KBr pellets. FT Far-IR spectra have been recorded with a Nicolet 20F FT-IR spectrometer (650-50 cm^{-1}) with a TGS (room temperature) detector using polyethylene wafers. Electronic absorption spectra were measured in methanol solution using a Perkin-Elmer 550 S spectrophotometer [16,17]. The potentiometric titrations and calculations of the stepwise dissociation constants in 75% (v/v) dioxane-water were performed as described earlier [18–20].

Films of HBDHT were prepared by utilizing POLOS spin coater. The films were studied by using a Shimadzu AFM. Photoluminescence attributes were measured utilizing RF-5301. Optical transmission and reflection were measured by utilizing JASCO 670 spectrophotometer in the spectral range 200–2500 nm. Single crystalline p-type Si (100) wafers were purchased from Nippon Mining Co. and etched by using the CP4 solution (HF: HNO_3: CH_3COOH with ratio 1:6:1). Current–voltage characteristics of the heterojunction were measured by means of high impedance electrometer type Keithley 2635 A. Illumination of the heterojunction was accomplished by utilizing a white halogen tungsten with intensity measured utilizing a TM-206 solar power meter.

2.1.1. Synthesis of 5, 6 di phenyl-3-hydrazino-1, 2, 4-triazine (DHT)

A mixture of 5,6 diphenyl-3-chloro-1,2,4-triazine(1 gm) and hydrazine hydrate (99%) anhydrous (2 ml), was heated under reflux for one hour, the reaction product was cooled then the greenish precipitate collect and re-crystallized from ethanol, m. p. 172 °C.

2.1.2. Synthesis of 2-benzylidene-3-hydroxy-1-(5,6-diphenyl-1,2,4-triazine-3-yl)hydrazine (HBDHT)

A mixture of an ethanolic solution of DHT and the stoichiometric amount of salicyaldhyde in ethanol was refluxed for one hour. The yellow crystals obtained were filtered off, washed with ethanol and re-crystallized from dichloroethane and stored over silica gel, m. p. 267 °C. Anal. Calcd. For HBDHT, $C_{22}H_{17}N_5O$: C 71.90%, H 4.63% and N 19.00%; experimentally: C 70.90%, H 4.80% and N 18.43%, these data showed good agreement with the proposed structure of HBDHT compound.

The FT-IR (Fig. 1): 3537 cm^{-1} ($\nu_{OH\ group}$), 3225 cm^{-1} (ν_{NH}), 1607 cm^{-1} ($\nu_{C=N}$) and 1508 cm^{-1} ($\nu_{C=C}$), 1455 cm^{-1} ($\nu_{(C=N)}$ triazine) and 818 cm^{-1} ($\nu_{C-\ N}$) triazine) [20]. In addition to several bands for triazine ring in the far-IR region at 545, 390, 296, 270 cm^{-1} [18]. The UV–Vis spectra of the present Schiff-base in methanol within the region 200–800 nm displays three bands at 500, 400 (n-π^* transition, R-band) and 235 nm (π–π^* transitions, K-band) [18,21–23]. The calculated dissociation constant (pK_a) values in 75% (v/v) dioxane-water at 25 °C of the current compound by potentiometric technique are12.43 ± 0.02 and 13.60 ± 0.0.8; corresponding to the hydroxyl and NH groups, respectively.

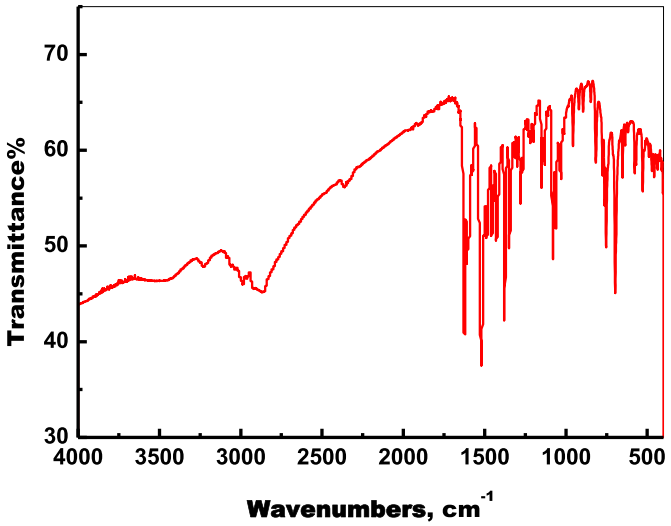

Fig. 1. FT- IR Spectrum of HBDHT compound.

3. Results and discussion

3.1. Morphology characterization

Surface morphology characterization of HBDHT was studied by using atomic force microscopy (AFM) and scanned for different areas to check for uniformity of the prepared films. AFM images of 2D and 3D directions are shown in Fig. 2 (a) and (b), respectively. As observed from the images, the morphology of the prepared films seems to be a column-like structure with different sizes and lengths. Besides, the AFM images indicate that all the films have a high roughness and high density of occupation of the columns all over the surface of substrates (i.e. nearly uniform). The obtained columns-like structure can particularly interesting for electronics and optoelectronic applications. The particle size was measured by using particle size analyzer and found to be 50 nm.

3.2. Optical characterization

Fig. 3(a) shows the spectral distribution of the HBDHT thin films in a wide range of 200–2500 nm of reflectance, R and transmittance, T. As observed, a fundamental transmission edge is observed which supporting for a suitable optical filter application. In addition, at longer wavelengths ($\lambda > 1000$ nm), the film become full transparency without any scattering or absorption (~$R + T = 1$). Nonetheless, at shorter wavelengths ($\lambda < 1000$ nm) the absorption by the film is taken place and then $R + T < 1$.

The absorption coefficient, α, can be calculated from T (λ) and R (λ) and film thickness d by using equation (1) [24–30]

$$\alpha = \frac{1}{d} \ln \left(\frac{(1-R)^2}{2T} + \sqrt{\frac{(1-R)^4}{4T^2} + R^2} \right) \quad (1)$$

The absorption coefficient of light influenced by several parameters such as: material type of the film, the film thickness, optical conductivity and extinction coefficient of the film as well as skin effect or skin thickness. Moreover, the skin depth can be influenced by both the film conductivity and the incident photons frequency and related to α according to expression 2 [24].

$$\delta = \frac{1}{\alpha} \quad (2)$$

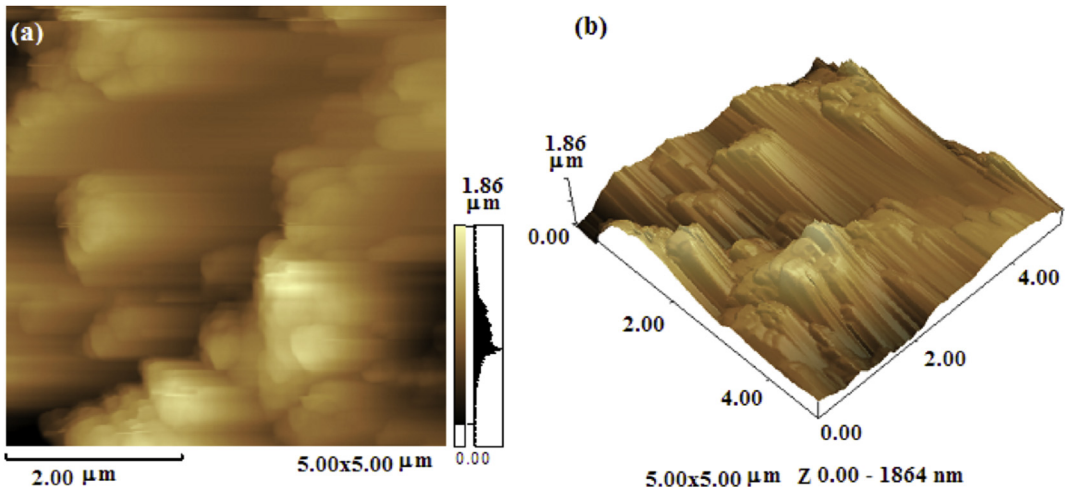

Fig. 2. Atomic force microscopy image (a) 2D view and (b) 3D view of HBDHT thin films.

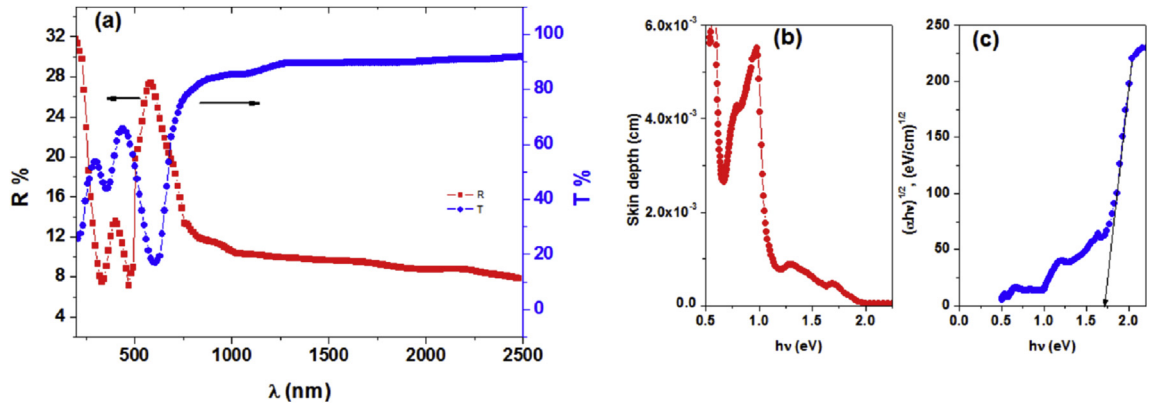

Fig. 3. (a) Spectral behavior of the reflectance R (λ) and transmittance T(λ), (b) plot of skin depth *vs.* hν and (c) Plot of $(\alpha h\nu)^{1/2}$ *vs.* hν of HBDHT film.

Fig. 3 (b) illustrates the dependence of δ on the photon energy (hν) for HBDHT thin films. As observed, δ increases with the increasing of the photon energy up to a certain value of the photon energy, 0.9 eV, then decreases and becomes zero at 1.90 eV, corresponding to λ = 653 nm (called cut-off value). For photon energy greater than this value, the absorption of the film for light vanishes and the reduction in amplitude is taken place after passing a large distance. The situations of the skin depth peaks and their intensities are dependent upon the type of the film.

The optical band gap of HBDHT thin films was extracted from the investigation of the absorption spectrum close to the principal absorption edge which is considered to be of type indirect allowed transition. Subsequently, the absorption coefficient can easily be obtained according to Tauc's relation for the allowed non-direct transition [25] by expression 3:

$$(\alpha h\nu)^{1/2} = K(h\nu - E_g), \tag{3}$$

where K is a constant related to the transition probability and E_g is the optical band gap. As observed, the best fitting of $(\alpha h\nu)^{1/2}$ *vs.* photon energy $(h\nu)$ for six is obtained (Fig. 3 (c)). The value of E_g was estimated from the intercept of $(\alpha h\nu)^{1/2}$ *vs.* $(h\nu)$ at $(\alpha h\nu)^{1/2} = 0$ according to the above equation and found to be 1.7 eV.The obtained value of energy gap indicates that HBDHT is expected to be best for photovoltaic consideration, and will have a higher efficiency in addition to several other advantages [26]. The obtained energy gap (1.7 eV) is too lower than those extracted from the molecular orbital calculations (6.28 eV).

The spectral dependence of the refractive index in the transparent region can be explained by the single oscillator model and expressed by Wemple and Di-Domenico to extract the main dispersion parameters as follows [27]:

$$\frac{1}{(n^2-1)} = \left(\frac{E_0}{E_d}\right) - \frac{1}{E_0 E_d}(h\nu)^2, \tag{4}$$

where $h\nu$ is the photon energy, E_d is the dispersion energy and E_0 is the single oscillator energy. A plot of $(n^2-1)^{-1}$ vs. $(h\nu)^2$ is illustrated in Fig. 4(a) for HBDHT thin film. Values of E_0 and E_d can easily be determined from the slope $(E_0E_d)^{-1}$ of the linear section of the curve and its intercept with the ordinate axis (E_0/E_d) and found to be 3.11 and 9.00 eV, respectively.

The real part of dielectric constant, ε_1, can be used to obtain the high-frequency dielectric constant and describe the lattice vibration modes of the dispersion using the relation given by equation (5) [28,29]:

$$\varepsilon = n^2 = \varepsilon_\infty - \left(\frac{e^2}{4\pi^2 c^2 \varepsilon_0}\frac{N}{m^*}\right)\lambda^2, \tag{5}$$

where ε_∞ is the high-frequency dielectric constant, ε_0 is permittivity of free space, N/m^* is the ratio of carrier concentration to its

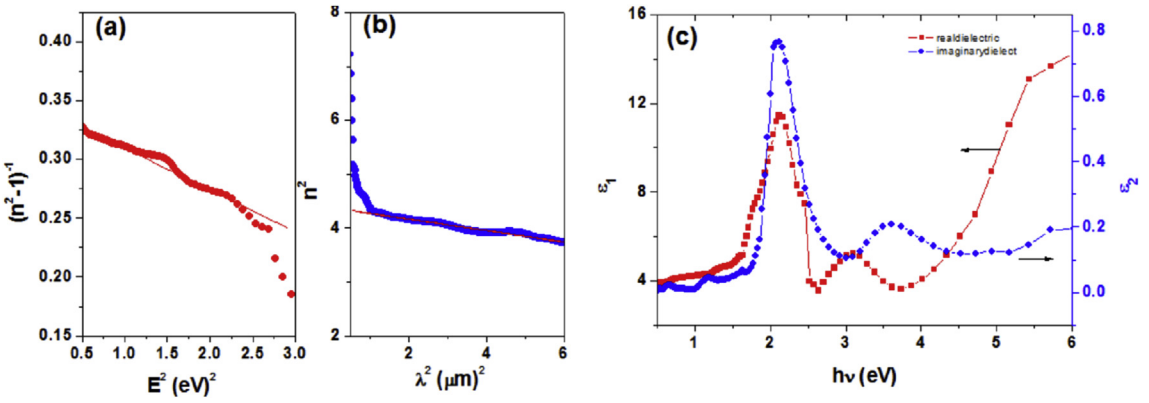

Fig. 4. (a) Plot of $(n^2\text{-}1)^{-1}$ *vs.* hν, (b) Plot of n^2 *vs.* λ^2 and (c) Photon energy dependence of ε_1 and ε_2 of HBDHT film.

effective mass and c is the velocity of light. The spectral distribution of n^2 *vs.* λ^2 is shown in Fig. 4(b). It is observed that n^2 decreases with increasing wavelength. At long wavelengths, the dependence of ε_1 on λ^2 is fitted to linear. The value of the high-frequency dielectric constant was determined from the extrapolation of the straight line section of the curve to intersect with the ordinate axis and found to be 4.37. The value of N/m^* was determined from the slope of the curve and found to be 1.22×10^{-57} kg/m^3. Real and imaginary parts of the complex dielectric constant,ε_1 and ε_2, respectively. The photon energy dependence of both ε_1 and ε_2 is shown in Fig. 4(c). As observed, ε_1 and ε_2 obey the same mode in the photon energy below 2.5 eV, corresponds to a peak at about 2 eV. After which the behavior is opposite, where a maximum of ε_2 corresponds to a minimum of ε_1. Furthermore, values of ε_1 are higher than those for ε_2. The variety of dielectric capacity with photon energy shows that a few interactions amongst photons and electrons in the film happen inside the studied energy range [30,31]. Similar behavior was observed for some organic thin films published by Ashery [32], Farag [33,34] and El-Nahass et al. [35,36].

3.3. Current–voltage characteristics

The *I-V* characteristics of HBDHT/p-Si heterojunction at room temperature (300 K) under dark condition are illustrated in Fig. 5(a). Good rectifying characteristics are observed, confirming the presence of a barrier between HBDHT and Si, and the forward diode current is found to increase exponentially with the applied voltage. Moreover, the rectification factor can easily be extracted from the ratio of the forward current to the reverse one at the same applied voltage (±1 V) and listed in Table 1. A higher value of rectification factor indicates a high execution of the heterojunction [37]. Accordingly, the prepared heterojunction behaves like as a diode. Therefore, the current–voltage characteristics can be expressed as follows [38,39]:

$$J = J_0\left(\exp\left(\frac{qV}{\eta kT}\right) - 1\right), \tag{6}$$

where V is the definite forward bias voltage, η is the ideality factor, k is the Boltzmann constant, T is the temperature, and the reverse saturation current density J_0 is determined by equation (7):

$$J_0 = AA^*T^2 \exp\left(\frac{-q\Phi_b}{kT}\right), \tag{7}$$

where A^* is the Richardson constant (32 A/cm^2 K^2 for p-type Si) [40] and Φ_b is the zero-bias barrier height as follows:

$$\Phi_b = \frac{kT}{q}\ln\left(\frac{A^*T^2}{J_0}\right) \tag{8}$$

In addition, the ideality factor can be determined from the *J-V* characteristics using relation 9:

$$\eta = \frac{q}{kT}\left(\frac{dV}{d\ln(J)}\right) \tag{9}$$

Taking the logarithm of Eq. (7), and using the plot of ln J *vs.* V

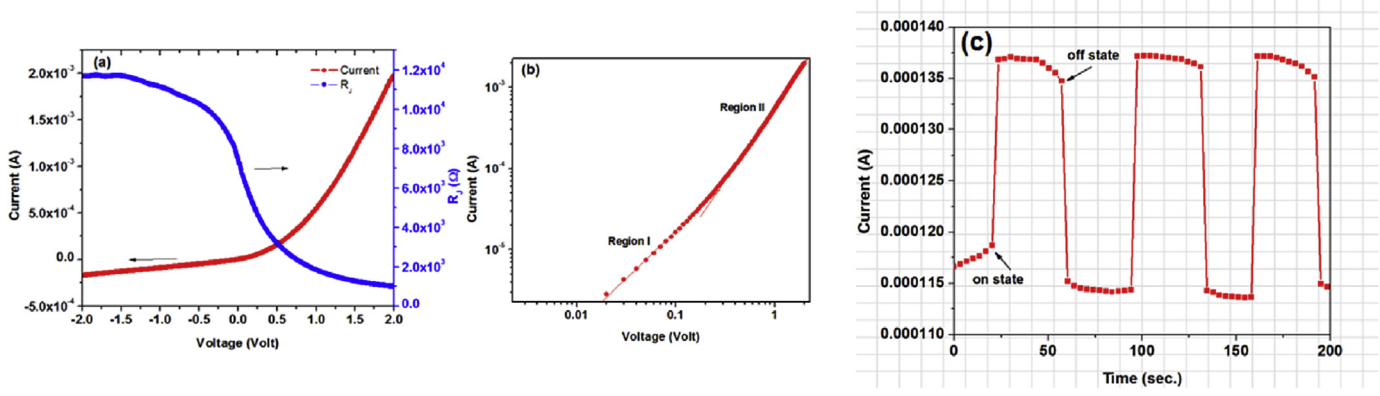

Fig. 5. (a) Current -voltage characteristics and R_J *vs.* Voltage of HBDHT/p-Si heterojunction, (b) Logarithmic current -voltage characteristics and (c) Plot of the transient photocurrent of HBDHT/p-Si heterojunction.

Table 1
Current –voltage parameters of *2-benzylidene-3-hydroxy -1-(5,6-diphenyl-1,2,4-triazine-3-yl)hydrazine* (HBDHT) based heterojunction.

Structure	RF	η	J_0(A)	Φ_b (eV)	R_s (Ω.cm^2)	R_{sh}(Ω.cm^2)	Reference
In/HBDHT/p-Si heterojunction	10	1.6	1.2×10^{-6}	0.75	10^3	1.2×10^4	Present work
Au/pyronine G(Y)/p-GaAs/Au:Zn	13	2.52	2.77×10^{-8}	0.69	510	1878	[45]
Au/Pyronine G(Y)/p-Si/Al	95.65	2.7	3×10^{-8}	0.83	2.32×10^3	–	[46]
Zn[$((NO_2)_2$-8HQ$)_2$]/p-Si	–	7.2	5.4×10^{-4}	0.63	50	760	[47]

(not shown here), one can obtain the reverse saturation current value and then the barrier height of the. In addition, the ideality factor can easily be obtained from the slope of the plot as discussed by Ajimsha et al. [39]. The estimated parameters of reverse saturation current, barrier height and the ideality factor, in comparison with those organic based heterojunction, are tabulated in Table 1. The basic parameters of the devices are compared to the conjugated organic devices. A higher value of the calculated ideality factor than unity was refer to that the operating conduction mechanism in our heterojunction could be quite realized by thermionic emission as discussed by Sharma and Purohit [40]. Vardhanan et al. [41] have attributed the higher ideality factor to the high prospect of recombination of charge carriers in the depletion region and/or the contribution of tunneling effect.

Another parameters affected the characteristics of the heterojunction are the series and shunt resistances. Salinas et al. [42] have attributed the importance of these resistances to that the series resistance is considered to be the summation of all resistances of the heterojunction (contact resistance, bulk resistance) while the shunt resistance can be attributed to leakage current under low bias. Accordingly, for ideal hetero-junction the series resistance tends to zero, while the shunt resistance tends to infinity as stated by Abdel Rafea et al. [43] and Farag [44]. Series and shunt resistances, in this study, can be estimated from the plot of junction resistance (R_J) versus the applied voltages (not shown here). The R_s value can be specified at high forward bias, where the junction resistance tends to a nearly constant. Furthermore, the shunt resistance can be extracted by the same method but at high reverse bias as discussed before by Soliman et al. [45]. The values of the series and shunt resistances were estimated, in comparison with those published organic based heterojunction, are tabulated in Table 1. As observed, a higher shunt resistance of the presented hetero-junction is comparatively better than to those published heterojunction [45–47].

To obtain information on the operative conduction mechanism of the presented heterojunction, double logarithmic characteristics are demonstrated in Fig. 5 (b). Using the power law of the I–V, $I \alpha V^m$ (m refers to exponent for identifying the operating mechanism. As observed, two linear –fitting regions were obtained indicating the presence of two operating conduction mechanism depending on the applied voltage region. In the first applied voltage region, m~1 indicating the prevalence of ohmic conduction mechanism. Under higher applied voltage, m~ 2 corresponding to the space charge conduction mechanism. The latter can be attributed to the occurrence of traps near the Fermi level of the layer in which SCLC is taken place. This behavior is in agreement with those published for various heterojunction [48–50].

The photo response properties of HBDHT/p-Si heterojunction at room temperature (300 K) under an illumination condition of 100 mW/cm^2 are illustrated in Fig. 5(c) by using photocurrent measurement. The dark and illuminated current was measured for a short time ~30 s and the current is measured versus time. Upon illumination, current values increase sharply from 1.15×10^{-4} A to 1.37×10^{-4} A. After which, the current decreases rapidly to its original value with highest able and reproducibility characteristic after the light is switched off. The current in the case of on-state/off-state (ratio of on-state/off-state) is found to be ~1.2. Although, the ratio of on-state/off-state is small as compared to other published for another hetero structures but it considered to be acceptable for application due to the reproducibility and sensitivity for illumination which suggests that the possibility for photo detector and application for optical switching [51,52].

3.4. Molecular orbital calculations

Molecular orbital calculations provide a definite depiction of orbitals including spatial attributes, nodal patterns, and individual atom contributions. Density function theory (DFT) calculations were performed to optimize the elucidated structure of present compound (HBHDT) at the B3LYP-6-31G level provided by the *Gaussian 09* program. Fig. 6 shows the optimized molecular structure of the most stable form of HBDHT. The contour plots of the frontier orbitals for the ground state of HBDHT is shown in Fig. 7, providing comparison of HOMO and LUMO. It is intriguing to see that both orbitals are significantly appropriated over the conjugation plane. The structural parameters data calculated of the studied compound are: total energy –1197a.u., heat of formation, ΔH (-850 kcal/mol), dipole moment (0.6351μ/D). The calculated data agree to that reported for the related compounds [53,54].

The frontier molecular orbitals play an important role in the electric and optical properties, as well as in UV–vis spectra and chemical reactions [54–56]. Fig. 7 illustrates the distributions and energy levels of the HOMO-1 (–0.2532), HOMO (–0.2324), LUMO (–0.0012) and LUMO+1(-0.0001) orbitals. The calculations indicate that the title compound has 95 occupied molecular orbitals. Both the HOMOs and LUMOs are basically localized on the rings indicating that the HOMO–LUMO is mostly the π-anti-bonding type orbitals [57]. Fig. 7 establishes that the HOMO-1 and HOMO orbitals are mainly delocalized on the triazine group, while the LUMO and LUMO+1 orbitals are mainly delocalized on triazine group and phenyl rings. The observed electron transitions can be assigned to the n-π* and π-π*electron transitions. The value of the energy separation between the HOMO and LUMO is 0.231a.u. (6.28 eV).

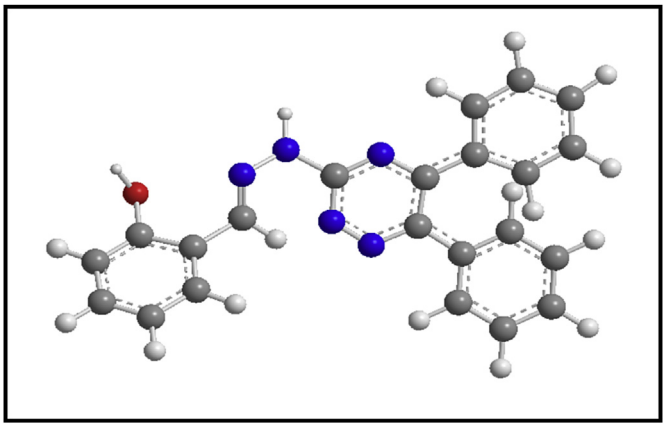

Fig. 6. Optimized structure of HBDHT compound.

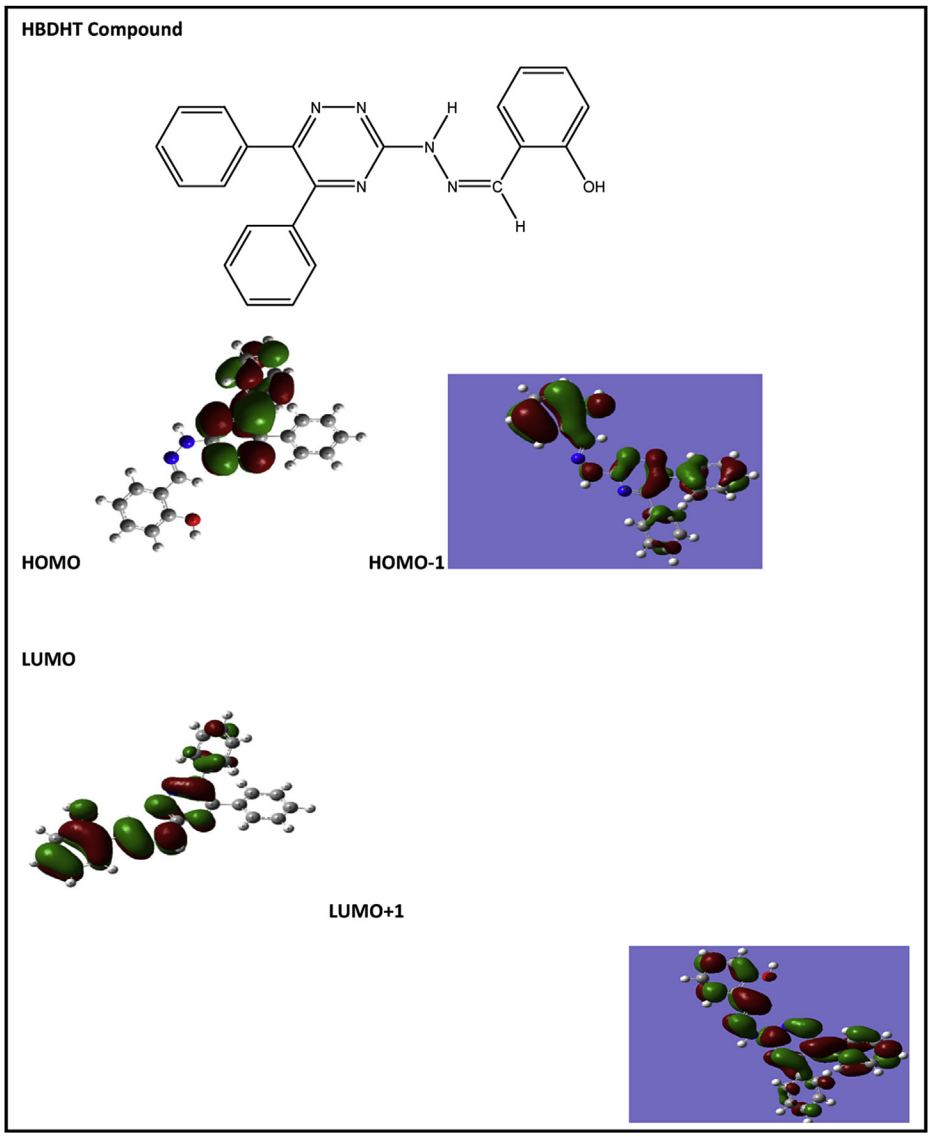

Fig. 7. Electron density of the highest occupied molecular orbital (HOMO) and the lowest unoccupied molecular orbital (LUMO) of HBDHT Compound.

This energy gap indicates that the HBDHT is potentially interesting electronic transitions as those involving narrow energy gaps.

4. Conclusions

In this work, the Schiff base, ***2-benzylidene-3-hydroxy -1-(5,6-diphenyl-1,2,4-triazine-3-yl)hydrazine*** (HBDHT) was successively synthesized and characterized by methods for different spectroscopic techniques and elemental analysis. Thin films of HBDHT films were prepared by spin-coating technique and exhibit well crystalline structure with a column -like structure of different sizes and lengths, supported by AFM. Fluorescence spectrum exhibits well defined strong greenish-blue emission band with wavelength 503 nm. The transmittance and reflectance spectra showed that the thinner film has the highest transparency. The optical characterization of the film indicated indirect allowed electronic inter-band transition and the optical band gap is found to be 1.70 eV. Current density −voltage characteristics dominates ohmic conduction at low voltages, whereas at high voltages, the process is dominated by the space charge conduction mechanism. Photocurrent characteristics of HBDHT/p-Si heterojunction show a significant sensitivity to light and then could be promising for optoelectronic device applications. Optimization the HBDHT structure was carried out by means of DFT molecular orbital calculation at the B3LYP-6-31G level provided by the *Gaussian 09* program. The optimized structure designated that the HOMO-1 and HOMO orbitals are mainly delocalized on the triazine group, while the LUMO and LUMO+1 orbitals are mainly delocalized on triazine group and phenyl rings. The calculated energy separation between the HOMO and LUMO in gaseous state is 6.28 eV indicated that the HBDHT is potentially interesting electronic transitions as those involving narrow energy gaps.

Acknowledgment

This work was carried out through the collaboration between some staff members of Department of Physics and Chemistry, Faculty of Education, Ain Shams University and Electronic Materials Department, Advanced Technologies and New Materials Institute, City for Scientific Research and Technology Applications.

References

[1] G. Wang, Z. Peng, J. Wang, X. Li, J. Li, Synthesis, molecular docking and α-glucosidase inhibition of 2-((5,6-diphenyl-1,2,4-triazin-3-Yl)thio)-N-arylacetamides, Eur. Med. Chem. 125 (2017) 423–429.

[2] L. Pavelek, V. Ladányi, M. Necas, Z. Moravec, K. Wichterle, Synthesis and characterization of lanthanide complexes with a pentadentate triazine-based ligand, Polyhedron 119 (2016) 134–141.

[3] J. Trifunović, V. Borčić, S. Vukmirović, M. Mikovm, Assessment of the pharmacokinetic profile of novel s-triazine derivatives and their potential use in treatment of Alzheimer's disease, Life Sci. 168 (2017) 1–6.

[4] P. Wen, X. Feng, Y. Kan, Y. Hu, R.K.K. Yuen, Synthesis of a novel triazine-based polymeric flame retardant and its application in polypropylene, Polym. Degrad. Stabil. 134 (2016) 202–210.

[5] K. Huthmacher, D. Most, Ullmann's Encyclopedia of Industrial Chemistry sixth ed., A10, Wiley-VCH, Weinheim, Germany, 2002, pp. 229–250.

[6] D.C. Sherrington, K.A. Taskinen, Self-assembly in synthetic macromolecular systems *via* multiple hydrogen bonding interactions, Chem. Soc. Rev. 30 (2001) 83–91.

[7] S.B. Holla, B.K. Sarojini, K. Shridhara, G. Antony, Synthesis of some New biologically active Thiadiazolotriazinones-Part III, II Farm. 54 (1999) 149–151.

[8] J. Ruiperez, M.A. Mendiola, M.T. Sevilla, J.R. Procopio, L. Hernandez, Electro Anal. 14 (2002) 532–539.

[9] B. Drazic, G. Popovic, R. Jelic, D. Sladic, D. Mitic, Z. Andelkovic, K. Tesic, Acid–base equilibria of the Zn(II) and Fe(III) complexes with condensation products of 2-acetylpyridine and the dihydrazide of oxalic and malonic acid, J. Serb. Chem. Soc. 74 (2009) 269–277.

[10] Y.A. Al-Soud, M.N. Al-Dweri, N.A. Al-Masoudi, Synthesis, antitumor and antiviral properties of some 1,2,4-triazole derivatives, II Farm. 59 (2004) 775–783.

[11] G.S. Gruzdyev, V.A. Zinchenko, V.A. Kalinin, R.I. Slovtsov, The Chemical Protection of Plants, Mir Publishers, Moscow, 1983.

[12] M. Moral, J.M. Granadino-Roldan, A. Garzon, G. Garcia, Manuel Fernandez-Gomez, in: 13rd International Conference of Synthetic Organic Chemistry, 1-30 Nov, 2009.

[13] G.B. Porter, V. Hanten, J. Inorg. Nucl.Chem. 18 (1979) 2053–2058.

[14] Organikum, VEB DeutscherVerlag der Wissenschaften, Berlin, 16thEdn, 1986.

[15] A.I. Vogel, Quantitative Inorganic Analysis, 4thEnd., Longman London, 1978.

[16] J.H. Yoe, A.L. Jones, Colorimetric determination of iron with disodium-1,2-dihydroxybenzene-3,5-disulfonate, Ind. Eng. Chem. Anal. 16 (1944) 111–115.

[17] V. Kapustianyk, M. Partyka, V. Rudyk, M. Piasecki, M.G. Brik, S. Tkaczyk, K. Ozga, K. Plucinski, S. Romanyshyn, I.V. Kityk, Spectroscopic studies of the size effects in the absorption spectra of $(NH_2(C_2H_5)_2)_2CuCl_4$ nanocrystals incorporated into the PMMA photopolymer matrix, J. Alloys Compd. 493 (2010) 26–30.

[18] D. Chapon, C. Husson, P. Delangle, C. Lebrun, P. J.A Vottéro, Solution properties of trivalent lanthanide trinuclear complexes with ligand 1,3,5-triamino-1,3,5-trideoxy-cis-inositol, J. Alloys Compd. 323–324 (2001) 128–132.

[19] H.M.N.H. Irving, U.S. Mohnot, pH-meter corrections for titrations in mixtures of water and dioxan, J. Inorg. Nucl.Chem. 30 (1968) 1215–1220.

[20] R. Shanmugakala, P. Tharmaraj, C.D. Sheela, C. Anitha, Synthesis and studies on S-triazine based ligand and its metal complexes, Int. J. Inorg. Chem. 2012 (2012) 1–7.

[21] P. Vouris, M. Freitag, V. Perebeinos, Carbon nanotube photonics and optoelectronics, Nat. Phot. 2 (2008) 341–350.

[22] A.A.T. Ramadan, M.A. El-Behairy, A.I. Ismail, M.M. Mahmoud, Synthesis and properties of iron(II) and iron(III) complexes with 3-(α,γ-dicarboxy-*n*-propylidene-hydrazino)-5,6-diphenyl-1,2,4-triazine (*DCPT*), Monatsh. Chem 125 (1994) 1171–1182.

[23] A.A.T. Ramadan, R.M. Abdel-Rahman, M.A. El-Behairy, A.I. Ismail, M.M. Mahmoud, The thermodynamics of complexation of transition and lanthanide ions by 3-(α-carboxymethylaminobenzyli-denehydrazino)-5,6-diphenyl-1,2,4 triazine (HipHt), Thermochim. Acta 222 (1992) 291–297.

[24] A.H. Ammar, A.A.M. Farag, M.S. Abo-Ghazala, Influence of Sb addition on the structural and optical characteristics of thermally vacuum evaporated Sb_xSe_{1-x} thin films, J. Alloys Compd. 694 (2017) 752–760.

[25] F. Urbach, The long-wavelength edge of photographic sensitivity and of the electronic absorption of solids, Phys. Rev. 92 (1953) 1324–1327.

[26] M. El-Hagary, M.E. Ismail, E.R. Shaaban, A. El-Taher, Effect of γ-irradiation exposure on optical properties of chalcogenide glasses $Se_{70}S_{30-x}Sb_x$ thin films, Rad. Phys. Chem. 81 (2012) 1572–1577.

[27] A.A. Abuelwafa, A. El-Denglawey, M. Dongol, M.M. El-Nahass, T. Soga, Structural and optical properties of nanocrystalline platinum octaethylporphyrin (PtOEP) thin films, J.Alloys Compd. 655 (2016) 415–422.

[28] A.S. Hassanien, A. Akl, Effect of Se addition on optical and electrical properties of chalcogenide CdSSe thin films, Superlattice Microstruct. 89 (2016) 153–169.

[29] A.S. Hassanien, Studies on dielectric properties, opto-electrical parameters and electronic polarizability of thermally evaporated amorphous $Cd_{50}S_{50-x}Se_x$ thin films, J. Alloys Compd. 671 (2016) 566–578.

[30] A. Ashery, A.A.M. Farag, M.A. Shenashen, Optical absorption and dispersion analysis based on single-oscillator model of polypyrrole (PPy) thin film, Synth. Met. 162 (2012) 1357–1363.

[31] O.I. Shpotyuk, R.Ya Golovchak, T.S. Kavetsky, A.P. Kovalskiy, M.M. Vakiv, Radiation–optical effects in glassy Ge–As(Sb)–S systems, Nucl. Instrum. Methods Phys. Res. B (2000), 517–167.

[32] P.O. Edward, Hand Book of Optical Constants of Solids, Academic press, New York, 1985.

[33] A.A.M. Farag, A. Ashery, M.A. Shenashen, Optical absorption and spectrophotometric studies on the optical constants and dielectric of poly (o-toluidine) (POT) films grown by spin coating deposition, Phys. B 407 (2012) 2404–2411.

[34] A.A.M. Farag, I.S. Yahia, Structural, absorption and optical dispersion characteristics of rhodamine B thin films prepared by drop casting technique, Opt. Commun. 283 (2010) 4310–4317.

[35] M.M. El-Nahass, Z. El-Gohary, H.S. Soliman, Structural and optical studies of thermally evaporated CoPc thin films, Opt. Laser Technol. 35 (2003) 523–531.

[36] M.M. El-Nahass, A.A. Atta, H.E.A. El-Sayed, E.F.M. El-Zaidia, Structural and optical properties of thermal evaporated magnesium phthalocyanine (MgPc) thin films, Appl. Surf. Sci. 254 (2008) 2458–2465.

[37] V.K. Sahu, P. Misra, R.S. Ajimsha, Amit K. Das, B. Singh, Effect of growth temperature on diode parameters of n-ZnO/p-Si heterojuction diodes grown by atomic layer deposition, Mater. Sci. Semicond. Proc. 54 (2016) 1–5.

[38] A. Hussain, Temperature dependent current–voltage and photovoltaic properties of chemically prepared (p)Si/(n)Bi2S3 heterojunction, Egypt. J. Basic Appl. Sci. 3 (2016) 314–321.

[39] R.S. Ajimsha, K.A. Vanaja, M.K. Jayaraj, P. Misra, L.M. Kukreja, Transparent p-AgCoO 2/n-ZnO diode heterojunction fabricated by pulsed laser deposition, Thin Solid Films 515 (2007) 7352–7356.

[40] B.I. Sharma, R.K. Purohit, Semiconductor heterojunctions, Pergamon press, Oxford, 1974.

[41] R.V. Vardhanan, L. Zhou, Z. Gao, Schottky and heterojunction diodes based on poly (3-octylthiophene) and poly (3-methylthiophene) films of high tensile strength, Thin Solid Films 350 (1999) 283–288.

[42] O.H. Salinas, C. Lopez-Mata, H. Hu, M.E. Nicho, Analysis of electrical parameters in heterojunctions based on poly 3-octylthiophene and cadmium sulfide thin films, Sol. Energy Mater. Sol. Cells 90 (2007) 2421–2428.

[43] M. Abdel Rafea, A.A.M. Farag, O. El-Shazly, E.F. El-Wahidy, N. Roushdy, Crystallite size estimation and photosensitivity characterization of nanocrystalline Zn_{1-x} Cd $_x$ S based heterojunctions prepared by simple dip-coating, Microelectron. Eng. 122 (2014) 40–45.

[44] A.A.M. Farag, Influence of temperature and illumination on the characteristics of nanocrystalline Ga0.29 Al0.71As based heterojunction prepared by MOCVD, J. Alloys Compd. 509 (2011) 8056–8064.

[45] H.S. Soliman, A.A.M. Farag, N.M. Khosifan, T.S. Solami, Electronic and photovoltaic properties of Au/pyronine G(Y)/p-GaAs/Au:Zn heterojunction, J. Alloys Compd. 530 (2012) 157–163.

[46] A.A.M. Farag, H.S. Soliman, A.A. Atta, Analysis of dark and photovoltaic characteristics of Au/Pyronine G(Y)/p-Si/Al heterojunction, Synth. Met. 161 (2012) 2759–2764.

[47] A.A.M. Farag, Sawsan M.S. Haggag, Mohamed E. Mahmoud, Thin film assembly of nano-sized Zn(II)-8-hydroxy-5,7-dinitroquinolate by using successive ion layer adsorption and reaction (SILAR) technique: characterization and optical–electrical–photovoltaic properties, Spectrochim. Acta Part A 93 (2012) 116–124.

[48] A.M. Farag, A. Ashery, F.S. Terra, G.M. Mahmoud, Investigations of Alsb thin films grown on Si by liquid phase epitaxy, J. Optoelectron. Adv. Matter. 10 (2008) 2713–2721.

[49] A. Turut, M. Saglam, H. Efeoglu, N. Yalcin, M. Yildirim, B. Abay, Interpreting the non-ideal reverse bias CV characteristics and importance of the dependence of Schottky barrier height on applied voltage, Phys. B 205 (1995) 41–50.

[50] A. Ashery, A.A.M. Farag, Mostafa Zeama, Structural,electrical and photo-transient characteristics of liquid phase epitaxial GaP based heterojunction for photodiode application, Superlattice Microstruct. 66 (2014) 136–147.

[51] F.A. Akgul, G. Akgul, H.H. Gullu, H.E. Unalan, R. Turan, Enhanced diode performance in cadmium telluride–silicon nanowire heterostructures, J. Alloys Compd. 644 (2015) 131–139.

[52] Q. Yang, K. Bergman, G.D. Hughes, F.G. Johnson, WDM packet routing for high capacity data networks, J. Light Wave Technol. 19 (2001) 1420–1426.

[53] R.C. Mehrotra, R. Bohra, Metal Carboxylates, Academic Press, New York, 1983.

[54] S.G. Baca, I.G. Filippova, O.A. Gherco, M. Gdaniec, YuA. Simonov, N.V. Gerbeleu, P. Franz, R. Basler, S. Decurtins, Zinc(II) complexes based on ortho-phthalic acid and ancillary N-Donor ligands, Inorg. Chim. Acta 357 (2004) 3419–3429.

[55] A.D. Becke, Density-functional thermochemistry. III. The role of exact exchange, J.Chem. Phys. 98 (1993) 5648–5652.

[56] C. Lee, W. Yang, R.G. Parr, Development of the Colle-Salvetti correlation-energy formula into a functional of the electron density, Phys. Rev. B 37 (1988) 785–789.

[57] M.J. Frisch, et al., Gaussian 03 Revision E.01, Gaussian Inc., Wallingford CT, 2004.